New geoelectrical characterization of a continental collision zone in the Central – Eastern Pyrenees: Constraints from 3-D joint inversion of electromagnetic data

Joan Campanyà[1,*], Juanjo Ledo[1], Pilar Queralt[1], Alex Marcuello[1], Josep Anton Muñoz[1], Montserrat Liesa[2], Alan G. Jones[3, +]

[1]Geomodels Research Institute, Dept. Dinàmica de la Terra i de l'Oceà, Universitat de Barcelona, Barcelona, Spain.

[2]Departament de Mineralogia, Petrologia i Geologia Aplicada, Universitat de Barcelona, Barcelona, Spain.

[3]Dublin Institute for Advanced Studies (DIAS), Dublin, Ireland.

[*] Now at School of Physics, Trinity College Dublin, Dublin, Ireland

[+] Now at Complete MT Solutions, Ottawa, Canada

Contact email: joan.campanya@tcd.ie

Keywords: Continental Collision; Pyrenees; Lithosphere; Lithosphere-asthenosphere boundary; Electromagnetic Geophysics; Joint inversion.

ABSTRACT

Continent-continent collisions are responsible for the formation of large mountain ranges like the Himalayas and the Alps and play a primary role in the development of the continents. The continental collision between the Iberian and European plates during the Alpine Orogeny resulted in the formation of the Pyrenees. In this study new electromagnetic data from the Eastern Pyrenees were complemented with older data from the Central Pyrenees, constraining the physical and geological processes at the eastern end of the Pyrenean mountain range. The electrical resistivity distribution beneath the Central-Eastern Pyrenees was characterized by means of three-dimensional (3-D) joint inversion of three electromagnetic datasets: (1) the MT impedance tensor (***Z***), (2) the geomagnetic transfer function (***T***), and (3) the inter-station horizontal magnetic transfer function (***H***). The main finding was the non-continuity to the east of the major conductive anomaly observed previously beneath the Central and West-Central Pyrenees related to partial melting of the Iberian subducted lower crust. Lower amounts of water (related to the presence of muscovite and biotite) in the subducted lower crust beneath the Eastern Pyrenees were suggested to explain the lack of partial melting in this part of the mountain range. The electrical resistivity model also revealed higher electrical resistivity values for the lithospheric mantle beneath the Eastern Pyrenees than beneath the Central Pyrenees, thus supporting the hypothesis of an heterogeneous Iberian plate inherited from the Variscan Orogeny. A less clear signature was the lateral variation along the strike direction of the lithosphere-asthenosphere boundary beneath the Eastern Pyrenees (relatively flat, between 110 km and 140 km depth) and the Central Pyrenees (north dipping, between 80 km and 120 km depth beneath the Iberian Plate and between 110 km and 160 km depth beneath the European plate), supporting the hypothesis of a missing lithospheric root beneath the Eastern Pyrenees.

1. Introduction

Tectonic processes dominate the development of the outermost layer of the Earth, and mapping them provides a great opportunity for Earth scientists to study and understand the dynamics and properties of the lithosphere. Continent-continent collision is a fundamental tectonic process that plays a primary role in the development of continents. The Pyrenean range resulted from the late Cretaceous to early Miocene continental collision between the Iberian and European plates, causing the subduction of the Iberian lower crust below the European crust (for a comprehensive geological review, see Muñoz, 2002). Our understanding of the geological and geophysical process that take place in the Pyrenees has been greatly aided by large geophysical datasets that have provided spectacular images of the subducted Iberian lower crust (IBSLC) below the Western and Central Pyrenees (e.g., Campanyà, 2013; Chevrot et al. 2015; Ledo et al., 2000; Macquet et al., 2014; Muñoz, 1992; Pous et al., 1995a; Teixell, 1998). Subduction of the Iberian lower crust below the European crust is currently accepted, and although several studies agree with the presence of partial melting associated with the IBSLC (Campanyà et al., 2011; Campanyà et al., 2012; Glover et al. 2000, Ledo et al, 2000; Pous et al., 1995b), other results support the hypothesis of aqueous fluids for explaining the observed geophysical anomalies (Vacher and Souriau, 2001; Souriau et al., 2008). In both hypothesis the dehydration process within the IBSLC is accepted, but differences appear when considering if the dehydration process can induce or not partial melting.

One of the problems for the understanding of the Pyrenean orogenic system concerns the crustal and lithospheric structures of the eastern termination of the Pyrenees and its transition to the western Mediterranean Sea, with a major interest on the characterization of the continuation to the East of the Iberian subducted lower crust observed below the Central and

Western Pyrenees. At crustal levels, Pyrenean structures continue along the NE Corbières trending transfer zone and parallel to NE faults, such as the Cévennes, into the Languedoc-Provence to connect with the Alps (Arthaud and Séguret, 1981; Séranne et al., 1995; Stampfli and Hochard, 2009). In these areas Pyrenean structures have been reactivated and overprinted by the extensional faults related to the opening of the Gulf of Lion and separation of Corsica and Sardinia Since Late Oligocene. In addition, the eastern tip of the Pyrenees coincides with a system of NW-SE trending extensional faults at the transfer zone between the Gulf of Lion and the Valencia Trough (Roca et al., 1999). Geophysical studies based on seismic and gravity datasets have already imaged significant differences between central and eastern Pyrenees, suggesting crustal and lithospheric thinning as the Pyrenees approaches the Mediterranean Sea (e.g., Chevrot et al., 2014; Gallart et al., 2001; Gunnell et al., 2008; Gunnell et al., 2009; Macquet et al., 2014), and also supporting the hypothesis of orogenic collapse at the eastern part of the Pyrenean mountain range, providing geophysical evidence of a missing lithospheric root in this region (Gunnell et al., 2008).

The electromagnetic signature of continent–continent collision zones depends on the age of the collision and usually presents a major low electrical resistivity structure at crustal or upper-mantle depths associated with water, melt, sulphides or graphite (i.e. Wei et al., 2001; Türkoğlu et al., 2008; Martí et al., 2009; and Selway et al., 2009). In active and relatively active collision zones the low electrical resistivity structures observed at crustal and upper-mantle depths are commonly associated with the presence of fluids, and partial melting. The low electrical resistivity values associated with partial melting and fluids surrounded by higher electrical resistivity values associated with the crust and the upper mantle creates a large resistivity contrast that makes the MT method ideal for the detection and analysis of fluids and partial melting (for a more comprehensive review see Unsworth, 2010). Previous

MT studies in the Pyrenees already revealed a major zone with low electrical resistivity values below the West-Central and Central Pyrenees interpreted as at least 2.5% of partial melting of the IBSLC (Campanyà et al. 2012; Glover et al. 2000; Ledo et al., 2000, and Pous et al., 1995b). In this study, new electromagnetic data from the Eastern Pyrenees was complemented with old data from the Central Pyrenees MT profile to constrain the propagation to the east of the IBSLC and constrain the associated physical processes. Three types of electromagnetic data with different sensitivity to geoelectrical structures were interpreted through three-dimensional (3-D) joint inversion for a more accurate characterization of the subsurface. The new electrical resistivity model of the Central – Eastern Pyrenees, jointly with the latest results obtained in the Central and West-Central Pyrenees and the available geological and geophysical data help us to deepen our understanding about continental collisions and the related physical properties.

2. Geological setting

2.1 Tectonic evolution

The Pyrenees were formed during the convergence of the Iberian and European plates from Late Cretaceous to Middle Eocene times (Choukroune and ECORS Team, 1989; Olivet, 1996; Rosenbaum et al., 2002), having as a major feature the north-dipping subduction of the Iberian lower crust beneath the European crust (Muñoz, 1992). However, there are several tectonic episodes that are worth mentioning in order to understand the complexity of this region. First, the Variscan orogeny configured a zonation of the Iberian Peninsula into more internal zones dominated by high-grade metamorphic rocks and granites and external zones composed by low-grade metamorphic rocks and sedimentary rocks, also producing alterations in the Paleozoic basement of the Pyrenean mountain range. The second major

event was the Early Cretaceous rifting in the Pyrenean domain that resulted in the formation of oceanic crust in the western part of the Bay of Biscay and the formation of a V-shaped rift system with a decreasing amount of extension from west to east (Roca et al., 2011). Subsequently, the northward displacement of Iberia during the Late Mesozoic and Cenozoic (Rosenbaum et al., 2002) initiated the inversion of the Cretaceous extensional basins in the Late Cretaceous (Garrido and Ríos, 1972). Finally, the Pyrenees resulted from a major collision during the Paleogene, with the subduction of the Iberian lower crust and mantle, and the formation of a southward directed thick-skinned thrust system (Beaumont et al., 2000). Subsequent to the continental collision, the eastern end of the Pyrenees was also affected by the influence of Neogene Mediterranean rifting that spread through a wide region of Western Europe affecting the eastern end of the Pyrenees by means of a NW-SE extensional period (Baize et al., 2002; Roca and Guimerà, 1992). Nowadays, the Pyrenees extend from the western Mediterranean to the Atlantic Ocean along northeastern Iberia and southwestern France, and major lateral variations are observed in structural style along the mountain range, possibly caused by the presence of an older segmented rift system in continuation with the Bay of Biscay, and by the influence of the Variscan orogeny that affected the Paleozoic basement of the Iberian plate (Beaumont et al., 2000; Jammes et al., 2014; Muñoz, 2002; Roca et al., 2011).

2.2 Main geological units

The Pyrenees are defined as an asymmetrical, double-wedge continental belt (Beaumont et al., 2000). A southern thrust system developed on top of the subducted Iberian plate, whereas a northern thrust system developed on top of the European plate. From north to south the Pyrenean range (Figure 1) can be divided into five major units: 1) the Aquitaine retro-foreland basin (AB), related to the northern Pyrenean wedge; 2) the northern Pyrenean thrust

system (NPTS); 3) the Axial Zone of the chain (AZ), formed by basement rock units with the North Pyrenean Fault (NPF) as its northern edge; 4) the southern Pyrenean thrust system (SPTS); and 5) the Ebro Foreland Basin (EB) associated with the southern Pyrenean wedge (e.g., Muñoz, 1992; Vergés et al., 1995). This division is well recognized for the Western and Central Pyrenees, but the eastern end of the Pyrenees presents particular features. These particular features are associated with the influence of the posterior Neogene Mediterranean rifting, having major extensional normal faults, crustal and topographic uplift, and lithospheric thinning (e.g. Lacan and Ortuño, 2012; Verges et al., 2002). This extensional system was also associated with the volcanic activity produced by the extrusion of basaltic-basanitic lavas formed by partial melting of the asthenospheric mantle (Martí et al., 1992; Neuman et al., 1999) south of the Pyrenean range. This event took place during the last 12 Ma, having the latest volcanic episode occurring 11,000 years ago in the Garrotxa volcanic area (GVA, in Fig. 1) (e.g. Martí et al., 2011).

3. Previous geophysical studies

Several geophysical studies have been undertaken in the Pyrenees determining the dynamics and physical properties of the subsurface at crustal and lithospheric scale, such as density, seismic velocity, and electrical conductivity.

3.1 Topography, Bouguer anomaly, and Earthquake locations

The analysis by Lewis et al. (2000) based on topography, in agreement with geological and geophysical results, supports the hypothesis of crustal and lithospheric thinning as the Pyrenees approach the Mediterranean Sea. Gunnell et al. (2009; 2008) integrated topographic, gravity, geoid anomaly and heat flow data to characterize several features

associated with the eastern end of the Pyrenees, such as an anomalously high topography, the absence of the IBSLC observed below the Central Pyrenees, and a shallower LAB compared to the Central Pyrenees. These results were used to support the hypothesis of orogenic collapse at the East of the Pyrenean mountain range and missing lithospheric root beneath the Eastern Pyrenees.

A study based on GPS data and earthquake focal mechanisms carried out by Rigo et al. (2015) is in agreement with the idea of major lateral variations along the mountain range, showing that the distribution of earthquakes in the Pyrenees also changes along strike. In the westernmost part of the range the strongest seismicity is present to the north of the range, in the central part the seismicity is mostly concentrated beneath the axial part of the range, and in the easternmost part the seismicity shifts to the south and extends further beneath the Mediterranean Sea.

Although no major and destructive earthquakes have been detected in the Pyrenees in modern times, historical earthquakes with probable magnitudes as high as 6.0 and 6.5 have been inferred from a seismic sequence with intensity VII - IX in 1427-1428 in the Eastern Pyrenees near the Garrotxa volcanic area (GVA) (Briais et al. 1990; Perea, 2009).

3.2 Active Source Seismic profiling

Deep active source seismic profiles at the Central (ECORS) and the West-Central Pyrenees (ECORS Arzacq) (grey lines in Figure 1) show a N-S progressive thickening of the Iberian crust from 30 km to 50 km as it approaches the longitudinal axis of the mountain range, whereas the European crust remains quite constant at depths between 30 km and 35 km (Muñoz, 2002; Teixell, 1998). Seismic studies in the Western and Central Pyrenees

corroborate thickening and subduction of the Iberian crust beneath the European crust (Dagnières et al., 1989; Muñoz, 1992; Roure et al., 1989), however this configuration does not persist at the eastern end of the mountain range. Major seismic features at the transition between the Pyrenean range and the Mediterranean Sea were constrained by the on-shore and off-shore recording of seismic profiles (Gallart et al., 2001; Nercessian et al., 2001; Vidal et al., 1998). These results show a dramatic reduction of crustal thickness as the Pyrenees approach the Mediterranean Sea, suggesting that in some areas the Moho beneath the mountain range (at a depth of approximately 28 km) is at a shallower depth than beneath the Iberian plate (approximately 32 km). Depth values for the Moho of around 25 km were observed at the eastern limit of the Pyrenees, at the Mediterranean coast.

3.3 Seismic tomography

Seismic velocity models indicate the presence of a negative-velocity anomaly associated with the IBSLC between the Central and West-Central Pyrenees, but these velocity anomalies are not observed to the east of the Central Pyrenees, where a more complex scenario with strong contrasts between positive- and negative-velocity anomalies are observed (e.g., Chevrot et al., 2014; Souriau et al., 2008). The S-wave velocity model of the Pyrenees by Macquet et al. (2014) also shows negative velocity anomalies beneath the Axial Zone of the Pyrenees that can be associated with the IBSLC, but these anomalous velocities do not extend to the eastern end of the Pyrenean range.

The teleseismic P-to-S converted wave model suggested by Chevrot et al. (2015) has also imaged the subduction of the Iberian lower crust beneath the Central and West-Central Pyrenees, in agreement with previous studies, but no equivalent model has yet been published constraining the crustal structures beneath the Eastern Pyrenees.

3.4 Geoelectrical models

The most significant outcome from previous deep-probing electromagnetic studies using the magnetotelluric (MT) technique is the imaging of a low-resistivity anomaly observed beneath the Central and West-Central Pyrenees spatially associated with the IBSLC. This conductive anomaly supports the hypothesis of partial melting of the IBSLC caused by the dehydration process of muscovite and biotite during the thermal re-equilibration of the IBSLC (Campanyà et al., 2012; Campanyà et al, 2011; Glover et al. 2000; Ledo, 2000; Ledo, 1996; Pous et al., 1995b). Another major result was the low electrical resistivity values observed at the bottom of the models related to the asthenosphere. The top of this conductive region was used to define the electrical lithosphere-asthenosphere boundary (eLAB) below the Iberian and European plates suggesting a thicker European plate, close to the collision zone. Campanyà et al. (2012) and Campanyà (2013) also constrained major differences between the West-Central and Central Pyrenees, showing the dissimilar dip of the low-electrical resistivity structures associated with partial melting of the IBSLC (maximum dips of 80^{o} beneath the Central Pyrenees, and 35^{o} beneath the West-Central Pyrenees were observed). Note that despite the differences, the low electrical resistivity anomaly associated with partial melting of the IBSLC was observed below the West-Central and Central Pyrenees MT profiles.

4. Electromagnetic data

In this study three different types of electromagnetic data were interpreted to characterize the electrical resistivity values of the lithosphere below the Central-Eastern Pyrenees. The MT impedance tensor (***Z***) (Cantwell and Madden, 1960; Neves, 1957; Rokityanski, 1961), commonly used to determine the electrical resistivity values of the subsurface, was complemented by the less commonly used geomagnetic transfer function (***T***) (Parkinson,

1962; Wiese, 1962), and the very rarely used inter-station horizontal magnetic transfer function (***H***) (Berdichevsky et al., 1968; Egbert and Booker, 1989; Schmucker, 1970). The MT impedance tensor (***Z***) describes the linear relationship between the measured horizontal components of the electric (E_x, E_y) and magnetic (H_x, H_y) fields. The geomagnetic transfer function (***T***) describes the linear relationship between the vertical component of the magnetic field (H_z) and the horizontal components of the magnetic field (H_x, H_y). Although this dataset is not sensitive to the absolute electrical resistivity values, it is very sensitive to lateral resistivity contrasts (e.g. Siripunvaraporn & Egbert, 2009; Habibian & Oskooi, 2014). Finally, the inter-station horizontal magnetic transfer function (***H***) describes the linear relationship between the measured horizontal magnetic field at one site (H^1_x, H^1_y,) and the horizontal magnetic field measured at a different site (H^2_x, H^2_y). This dataset, which is also not sensitive to the absolute electrical resistivity values of the subsurface geology, also contributes to define lateral changes (e.g. Sokolova et al., 2007; Soyer and Brasse, 2001; Varentsov et al., 2015a,b). In the particular case of this study, the main motivation for using ***H*** was to improve the consistency of the model, as the data from the two profiles, independently on the distance between them, were directly related. The direct relation between data measured at different sites imposed by the ***H*** tensor forced the resistivity values below each profile to be consistent with the resistivity values below the other profile, increasing the credibility of the results when evaluating the lateral changes along the strike direction between the Central and Eastern Pyrenees MT profiles. For a more detailed description of the advantages of complementing ***Z*** with ***T*** and ***H*** responses see Campanyà et al. (2016).

New MT data were acquired in autumn 2010 at 13 sites along a 125 km profile crossing the Eastern Pyrenees (white stations marked on Fig. 1). Broadband magnetotelluric (BBMT) and

long period magnetotelluric (LMT) data were recorded at all sites. On average, the distance between sites was 10 km, and recording times were at least two nights for BBMT data, and twenty nights for LMT data. The BBMT data were recorded using Metronix ADU06 and ADU07 systems, acquiring horizontal electric and horizontal magnetic fields (no vertical magnetic field, Hz). BBMT data were processed using Metronix software (Friedrichs, 2003) to obtain $\boldsymbol{Z}$ responses. The LMT data were recorded using LEMI systems designed by Lviv Center of the Institute of Space Research, acquiring vertical magnetic, horizontal electric and horizontal magnetic fields. The LMT data were processed using the BIRRP algorithm (Chave and Thompson, 2004) to obtain $\boldsymbol{Z}$, $\boldsymbol{T}$ and $\boldsymbol{H}$ responses. Remote reference (RR) (Gamble et al., 1979a,b) and ELICIT (Campanyà et al., 2014) routines were performed when processing the data in order to avoid the effects of local noise and to improve the statistics. For BBMT data, RR was performed between sites that recorded simultaneously. For LMT data, RR and ELICIT were performed using the INTERMAGNET (www.intermagnet.org) magnetic fields from the Fürstenfeldbruck (FUR) and Chambon la Fôret (CLF) magnetic observatories, which are located at around 1000 km north-east and 600 km north of the study area, respectively. The use of data from magnetic observatories located at large distances from the area of study was recently supported by Neska et al. (2018), with the aim of reducing the effects of geomagnetic sources that could disturb the processing results and lead to miss-interpretation of the subsurface geology.

The presence of anthropogenic noise in the Eastern Pyrenees, mostly affecting the electric field measurements, makes the estimation of the MT impedance tensor difficult, in particular for the diagonal components, which being of lower amplitude are far more affected by the presence of noise. Only the off-diagonal components of $\boldsymbol{Z}$ from seven sites (out of thirteen) were used in this study, covering a period range between 0.01 s and 10000 s. This deficit was

solved by also using ***T*** and ***H*** responses recovered at thirteen and twelve sites respectively, covering a period range between 30 s and 10000 s. For the ***H*** responses, for which a reference site is required to compare the magnetic fields between two locations, site E2 (penultimate southernmost site on Eastern Profile, Fig. 1) was chosen as a neighbouring reference site. E2 was selected because is not located on top of strong geoelectrical anomalies, which facilitate the inversion process (Campanyà et al., 2016). The ***H*** and ***T*** responses were derived only for the LMT data, giving more weight to the periods affected by lithospheric-scale structures, and thus biasing the inversion to focus more on deep structures relative to shallower ones. An error floor was imposed for all data types for the dimensionality analysis and the inversion process. An error floor of 5% was imposed for all ***Z*** components, using 5% of $|Z_{xy}|$ for the Z_{xx} data and 5% of $|Z_{yx}|$ for the Z_{yy} data if the absolute value of the diagonal component was smaller than the absolute value of the off-diagonal component, respectively. Note that this approach assumes that the error is predominantly in the electric field. An absolute error floor of 0.03 was assumed for ***T*** and ***H*** responses.

Twenty-eight BBMT sites, eight of which also had LMT data (marked by larger orange circles, Fig. 1), from the Central Pyrenees acquired in 1994 and 2009, and already used to constrain the lithosphere below the Central Pyrenees (Campanyà et al., 2011; Ledo, 1996; Pous, 1995a) were also incorporated in this study to determine major variations along-strike between the Central and Eastern Pyrenees MT profiles. In this study, LMT data from the Central Pyrenees were re-processed to determine the ***T*** and ***H*** responses, following the same procedure as for the Eastern Pyrenees data. For the ***H*** responses of the Central Pyrenees MT profile the same site E2 was used as a reference site. As data from the Central and Eastern Pyrenees were recorded at different years, the ***H*** responses were calculated using the time series from the permanent magnetic observatories, and related to site E2 by following steps

analogous to the ones used in the ELICIT methodology (Campanyà et al., 2014). Note that for the ELICIT methodology inputs and outputs related by the transfer functions do not need to be acquired simultaneously if there are additional time series at a different location recording simultaneously with the inputs, and the outputs; for example the permanent magnetic observatories in INTERMAGNET.

Due to the complexity of the area and the difficulties in correctly characterizing galvanic distortion, in particular where the diagonal components of $\boldsymbol{Z}$ are poor in quality, no correction or compensation was applied to the data to account for galvanic distortion, which is a tractable problem in 2-D cases but is far less so in 3-D (see Jones, 2011). As a 3-D modeling approach was used to recover the electrical resistivity values of the subsurface with a fine discretization in the uppermost part of the model, it was expected that the model would not be significantly affected by near-surface galvanic distortion effects at the target depths (see, e.g., Farquharson and Craven, 2009; Meqbel et al., 2014; Sasaki and Meju, 2006;). In addition, the inversion of $\boldsymbol{T}$ and $\boldsymbol{H}$ responses, which are minimally affected by galvanic distortion of the electric fields (e.g., Chave and Jones, 1997; Chave and Smith, 1994), would decrease the susceptibility of the resulting model to galvanic effects.

The presence of the highly conductive Mediterranean Sea close to the area of study already indicates a 3-D geoelectrical environment. The performed dimensionality analysis (S1, Supplementary material) corroborates the need of a 3-D approach for modeling the subsurface at the eastern end of the Pyrenean range.

5. Three-dimensional electrical resistivity model

A 3-D inversion process was carried out to characterize the geoelectrical subsurface at lithospheric-scale. The derived electrical resistivity model was constrained by performing 3-D joint inversion of ***Z***, ***T*** and ***H*** responses using the ModEM algorithm (Egbert and Kelbert 2012, Kelbert et al., 2014) with the incorporation of the ***H*** responses, thus improving the capability and accuracy of the inversion process in recovering the electrical resistivity structures (Campanyà et al., 2016).

The 3-D solution mesh comprised 110 x 104 x 113 cells in the north-south, east-west and vertical directions respectively. The core of the mesh comprised 82 x 76 x 113 cells with a horizontal cell size of 4 x 4 km, ensuring the presence of free cells between the sites. The lateral extent of the padding cells increased by a factor of 1.3. Topography and bathymetry were included and the electrical resistivity of the Atlantic Ocean and the Mediterranean Sea was fixed at 0.3 ohm·m. The thickness of the layers was 200 m for the cells with topography and bathymetry and then 400 m, increasing by a factor of 1.03 for subsequent layers in the z-direction, ensuring that at the greatest depth of interest, ~150 km, the vertical cell size was equal or smaller than the horizontal cell size.

Several preliminary inversions of the ***Z***+***T***+***H*** responses were executed to choose the initial electrical resistivity model and the regularization parameters. Values between 50 ohm·m and 500 ohm·m were tested for the initial homogeneous half space using smoothing values of 0.3 in all directions. Those results with poor fit to the data were excluded and the electrical resistivity value for the homogeneous starting model was chosen within a range of starting models that best fit the data. The final regularization parameters were chosen after additional tests were conducted inverting ***Z***+***T***+***H***. Several combinations of horizontal and vertical smoothing parameters were applied using smoothing values between 0.1 and 0.6 (always

assuming the same smoothing values for north-south and east-west directions). The largest smoothing parameters that fit the data were chosen for the inversion process to avoid the presence of artefacts generated by the inversion process.

Based on these tests, the chosen starting model was a homogeneous half-space of 110 ohm·m, and the smoothing values were 0.3 for north-south and east-west directions, and 0.2 for the vertical direction. It should be noted that after the first inversion results, following the same procedure as applied in Blake et al. (2016), a new initial model was created by averaging the initial half space model and the MT model derived from the inversion. This new initial model, containing the main electrical resistivity structures but without sharp contrasts in resistivity, was used as the initial model for the final inversion run. Results from the inversion process and the normalized root mean square misfit (nRMS) at each site and for each type of data are presented in Fig. 2 and Fig. 3. For a more detail evaluating the fit of the data, Fig. S2 in the supporting material shows the data and model responses in pseudosection format, and Fig. S3 the differences between data and model responses divided by the error in pseudosection format for each data type, site, and period.

5.1 Electrical resistivity structures

The main geoelectrical features are labeled *L* (Fig. 2a). The model contains four main geoelectrical structures. *L1* is associated with the IBSLC below the Central Pyrenees and with the presence of partial melting, already observed in previous MT studies. *L2* and *L3* towards the bottom of the model are associated with the asthenosphere below the Central and Eastern Pyrenees MT profiles, and its top with the eLAB. *L4* is related to the decrease in resistivity observed in the Iberian crust beneath the Eastern Pyrenees. The high-resistivity

values on top of *L2* and *L3*, up to ~35 km depth, are related to the lithospheric mantle beneath the Central and Eastern Pyrenees.

At shallower depths, down to 30 - 35 km, the presence of high electrical resistivity values are mostly associated with crystalline rocks at crustal depths, and the conductive anomalies with sedimentary basins (e.g. Ebro and Aquitaine Basin, EB and AB in Fig. 1) and major crustal faults. Authors would like to note that careful need to be taken when considering off-profile anomalies, such as A1 and A2 in Fig. 3. Even if the data acquired along the MT profiles may be sensitive to these anomalies, as no sites are located on top of the off-profile anomalies they cannot be recovered with a reasonable level of accuracy.

5.2 Non-linear sensitivity tests

Non-linear sensitivity tests were performed to justify the presence of the geoelectrical structures and appraise the resolution of the MT data and the validity of the resistivity model. The test consisted of comparing the final MT model with a modified model where some of the properties of the studied features were modified, such as the electrical resistivity values and the top of the anomalies (e.g. Ledo and Jones, 2005). Forward responses of the modified model and the final model were compared and the differences divided by the assumed errors during the inversion process. Alterations in the model that produced differences smaller than the assumed errors per each period and site, for all data types, were accepted as indicating that the model resolution inherent in the data was not sufficient to differentiate between the two models. Otherwise the modifications were not accepted.

Firstly, the requirement of the main geoelectrical structures recovered by the inversion process was examined. These structures were removed by replacing their electrical resistivity values with the electrical resistivity values of the surrounding blocks. Fig. S4 show the sites

and periods that are sensitive to the defined geoelectrical structures, supporting the necessity of these structures to fit the data. Note that different periods, components, and sites are sensitive to the same geoelectrical structure depending on the type of data, which emphasize the importance and advantages of performing joint inversion of $\boldsymbol{Z}$, $\boldsymbol{T}$ and $\boldsymbol{H}$, instead of only looking at the commonly used MT impedance tensor ($\boldsymbol{Z}$).

Secondly, the sensitivity test was applied to constrain the resolution at characterizing these structures. The sensitivity test showed that the electrical resistivity values of L1 could range between 3 ohm·m and 25 ohm·m. The performed tests also showed that this structure is only allowed few km to the east of the Central Pyrenees MT profile (Fig. 3, white solid-line rectangles). The electrical resistivity values of L2 and L3, at the bottom of the profiles, can range between 70 ohm·m and 100 ohm·m, with a larger range to the south of the Central Pyrenees profile, between 30 ohm·m and 100 ohm·m. Several tests were performed to determine the depth of the eLAB assuming electrical resistivity values for the asthenosphere between the observed ranges. In the Central profile, the top of the L2 can be located between 80 km and 120 km beneath the Iberian plate, and between 110 km and 160 km beneath the European plate. Note that an additional test with a flat boundary at 115 km depth did not agree with the responses at the surface, supporting the hypothesis of a north-dipping eLAB below the Central Pyrenees. Beneath the Eastern Pyrenees, the sensitivity test suggests a relatively flat eLAB along the North-South direction constraining the top of L3 at depths between 110 km and 140 km depth. Looking at the L4 structure, the electrical resistivity values can range between 100 ohm·m and 250 ohm·m, accepting a range of values always lower than the neighboring values at a similar depths (> 400 ohm·m).

An additional test was performed to show that the lithospheric mantle cannot be defined using constant electrical resistivity values (Figs. S4e, S4f), which indicates the need for an assumption of vertical variation with larger resistivity values at the top relative to the bottom. Note that the electrical resistivity values of the lithospheric mantle beneath the Eastern Pyrenees are higher than beneath the Central Pyrenees.

Finally, a sensitivity test was performed for the two off-profile anomalies labeled *A1* and *A2* (marked on Fig. 3, 20 km depth), testing if they were necessary to fit the data (Figs. S4g, S4h). In both cases the structures were required, particularly structure *A2* that has a strong influence on the profile to the East. Note that although our dataset is sensitive to *A1* and *A2*, because no data were acquired in these regions we are only able to resolve the associated geoelectrical structures or perform and adequate interpretation of these anomalies.

6. Discussion

The main results of the provided electrical resistivity model is the lack of appearance below the Eastern Pyrenees MT profile of the main conductive anomaly observed beneath the West-Central and Central Pyrenees related to partial melting of the IBSLC. In contrast to the Central and West-Central Pyrenees MT profiles, below the Eastern Pyrenees MT profile the subducted lower crust has higher electrical resistivity values than the surrounding lithospheric mantle, showing major lateral variations along the strike direction between the Central and Eastern Pyrenees MT profiles. The higher electrical resistivity values of the lithospheric mantle below the Eastern Pyrenees compared to the Central Pyrenees MT profile, and the dissimilarity between the eLAB beneath the Eastern Pyrenees MT profile and the eLAB beneath the Central Pyrenees MT profile highlight the presence of significant lateral changes between these two regions at lithospheric scale.

An analysis of the main geoelectrical features is presented below with reference to results from previous studies. Topography, Bouguer anomaly, and locations of earthquakes provided by the Institut Cartogràfic i Geològic de Catalunya (ICGC) were incorporated with the MT model (Fig. 4) to facilitate its interpretation. The depths of the eLAB, yellow dashed lines in Figure 4c, were constrained by the sensitivity test performed when defining the top of L2 and L3. In the Central Pyrenees MT profile we added a geological interpretation from Muñoz (1992) based on ECORS-Pyrenees deep seismic profile (ECORSPyrenees team, 1988; Choukroune and ECORS-Pyrenees Team, 1989), black lines, and in the Eastern Pyrenees MT profile we also superimposed the deeper structures from the same interpretation to facilitate comparison with the Central Pyrenees MT profile, black dashed lines. The NPF was used as a reference to locate the geological interpretation of the Central Pyrenees below the Eastern Pyrenees MT profile.

6.1 Iberian subducted lower crust (IBSLC), anomaly *L1*

The L1 structure beneath the Central Pyrenees is in agreement with previous MT studies that related this anomaly to the IBSLC and inferred the presence of partial melting (e.g. Campanyà, 2013; Ledo, 1996; Pous et al., 1995b). The obtained results were also compared with the proposed geological models of the area (Fig. 4c) and some seismic results (Fig. 5).

The new electrical resistivity model shows few differences associated with L1 in relation to the previous MT models. In particular, in the new electrical resistivity model L1 seems to be more vertically elongated and slightly more northerly located. In addition, the performed sensitivity test constrains the range of values for L1 between 3 ohm·m and 25 ohm·m, instead of between 3 ohm·m and 6 ohm·m as suggested by Campanyà et al (2011) from the 2-D

resistivity model, thus extending the upper range of possible resistivity values. The observed differences at constraining and defining this conductive structure are probably due to the improved approaches adopted in this study, such as the use of 3-D inversion, and the joint inversion of three different types of electromagnetic datasets (***Z***+***T***+***H***). As the IBSLC was already constrained by previous MT studies beneath the Central Pyrenees, the main contribution from this study is the characterization of the eastern end of the L1 anomaly. The provided results show that this anomaly can only be extended few kilometres to the east of the Central Pyrenees MT profile (white solid-line rectangles in Fig. 3 and that it is not allowed below the Eastern Pyrenees MT profile (white dashed-line rectangles in Fig. 3). If similar crustal structures are expected below the Eastern Pyrenees MT profile as in the Central Pyrenees (Fig. 4c, black dashed lines), in the Eastern Pyrenees the region associated with the IBSLC is characterized by high electrical resistivity values, higher than the surrounding values for the lithospheric mantle, showing a significant contrast along the strike direction between the two MT profiles (Fig. 4c).

Comparison with seismic results shows relatively good agreement between seismic and electrical resistivity models, although few discrepancies were also observed. The tomographic study of the Pyrenees from Chevrot et al., 2014 (Fig. 5a) also shows a significant contrast along the strike direction when comparing P-velocity values between Central and Eastern Pyrenees MT profiles, presenting a high velocity anomaly between Central and the Eastern Pyrenees MT profiles. Although this pattern is equivalent to the changes observed from MT results, having high electrical resistivity values east of the Central Pyrenees and beneath the Eastern Pyrenees MT profile, the high velocity region seems to be shifted to the west when comparing with the region with high electrical resistivity values. However, a more detailed analysis should be performed before getting

further conclusions evaluating if the observed differences are due to the physical properties of the subsurface geology or due to comparison between two methods with different levels of resolution. The Common Conversion Point (CCP) stack section from Chevrot et al., 2015 (Fig. 5b) in the Central Pyrenees shows a good agreement between the location of the low electrical resistivity anomaly associated with partial melting of the IBSLC, L1, (Fig. 5b, green dashed line) and the subduction of the Iberian lower crust imaged by seismic data (Fig. 5b, black-dashed lines represent the Moho). Unfortunately no equivalent seismic results are yet presented for the Eastern Pyrenees.

In the Central Pyrenees the partial melting of the IBSLC wasn't associated with anomalous high temperatures, but with the dehydration process of muscovite. Muscovite dehydration melting takes place at temperatures near the granite wet solidus at ~630 ºC. This reaction releases a small amount of melt, which does not migrate, as the critical melt percentage is not achieved. Extensive melting only occurs at temperatures over 800ºC, generally associated with dehydration-melting reactions of biotite, which was suggested below the West-Central Pyrenees MT profile at depths deeper than 60 km depth (Campanyà et al., 2012). The deeper levels outcropping in the North Pyrenean and Axial Zone suggest that the Pyrenean middle and lower crust is formed by pelites and greywackes metamorphosed during Variscan orogeny to amphibolite and granulite facies (Vielzeuf, 1984). Thus, the rocks can contain a limited amount of water in their structures stored in the hydrous phases, mainly in muscovite and biotite at lower temperatures (amphibolite facies) and biotite at higher temperatures (granulite facies). This means that the partial melting observed below the West-Central and Central Pyrenees can't be justified without the dehydration melting process caused by the presence of muscovite and biotite in the IBSLC. The absence of partial melting in the IBSLC below the Eastern Pyrenees MT profile can be justified by an heterogeneous Iberian lower

crust inherited from the Variscan orogeny. Thus, in the Eastern Pyrenees Variscan basement rocks have higher metamorphic grade and granulites and granites crop out, whereas towards the Central Pyrenees lower grade metamorphic rocks and un-metamorphosed basement rocks abound. This is in agreement with more dehydrated rocks towards the East and, consequently, less partial melt.

Previous studies from different geophysical datasets also show significant lateral contrast at the eastern end of the Pyrenean range, and suggest the absence of the subducted lower crust at the point where the Pyrenees meets the Mediterranean Sea (Chevrot et al., 2014; Gallart et al. 2001; Gunnell et al., 2009; Lewis et al., 2000; Macquet et al., 2014; Souriau et al. 2008). Note however that although there is the absence of the conductive anomaly beneath the Eastern Pyrenees MT profile, in this region there is still high topography, a decrease of the Bouguer anomaly, and seismic activity is observed at depths around 20 – 30 km depth (Fig. 4a,c), which suggest that the Iberian subducted lower crust is still present below the Eastern Pyrenees MT profile, although no presence of partial melting is observed in this region.

6.2 Lithospheric mantle electrical resistivity values

The horizontal slices at different depths (Fig. 3) show a contrast associated with the transition between the Central and the Eastern Pyrenees MT profiles at lithospheric upper-mantle depths, with slightly higher electrical resistivity values beneath the Eastern than the Central Pyrenees MT profile. These two areas with different electrical resistivity values define a NE-SW oriented contrast that can be related to the oblique orientation of the Variscan structures that were inherited before the continental collision, also supporting the hypothesis of an heterogeneous Iberian plate.

The electrical resistivity values of the lithospheric mantle are highly sensitive to parameters that characterize the thermal and compositional state of the lithosphere, and MT studies can be particularly helpful for constraining the amount of water in the lithospheric mantle. Low presence of water and low temperatures are commonly related to a lithospheric mantle with high electrical resistivity values, and large amounts of water and high temperatures are to a lithospheric mantle with low electrical resistivity values (for a comprehensive review see Fullea, 2017). Because of the proximity of the eastern Pyrenees to the Mediterranean Sea, where the asthenosphere is at shallower depths and similar or higher temperatures as in the Central Pyrenees are expected at the eastern end of the Pyrenean range, we assume that the changes in resistivity between the Central and Eastern Pyrenees MT profiles are caused by different composition of the lithospheric mantle and by a significant decrease in the content of water in the lithospheric mantle below the Eastern Pyrenees, which supports the idea of a heterogeneous Iberian plate due to the Variscan Orogeny with less amount of water to the East.

6.3 Lithosphere-asthenosphere boundary (LAB), *L2* and *L3*

The constrained eLAB from the electrical resistivity models and the non-linear sensitivity test is in agreement with an LAB that varies along-strike direction. The non-linear sensitivity test requires a north-dipping LAB beneath the Central Pyrenees MT profile, at depths between 80 km and 120 km beneath the Iberian plate and between 110 km and 160 km beneath the European plate, while a relatively flat LAB beneath the Eastern Pyrenees MT profile at depths between 110 km and 140 km is in agreement with the acquired electromagnetic data. The fact that the north dipping of the LAB is not required below the Eastern Pyrenees MT profile would be in agreement with the hypothesis of orogenic collapse by thermal erosion of

the Iberian lithospheric root, or lithospheric slab detachment, below the eastern end of the Pyreneean range, gradually propagating to the Central Pyrenees (e.g. Gunnell et al., 2009; Gunnell et al., 2008; Lacan and Ortuño, 2012). Because no significant intrusion of low electrical resistivity values is observed in the upper mantle associated with a possible slab break off, such as in the northern Gibraltar Arc (Rosell et al., 2011), the hypothesis of thermal re-equilibration and orogenic collapse affecting the eastern end of the Pyrenean range would be in better agreement with the observed MT results. Orogenic collapse only affecting part of the mountain range is also observed in the nearby Alps, in which the orogenic collapse is observed in the West Alps but not in the Central or East Alps (Selverstone, 2005).

6.4 Lithospheric-scale structure associated with previous volcanic activity, *L4*

The weak *L4* anomaly located beneath the Eastern Pyrenees, south of the Pyrenean range at mid-to-lower crustal depths, is a vertical low-resistivity region that at shallower depths diverges to the south through the Garrotxa volcanic area (GVA in Fig.1). This area is also coincident with a drop in topography (Fig. 4a) and it is slightly less populated by earthquakes than the adjacent regions (Fig. 4c). Although L4 was constrained by the sensitivity test, the resolution from the provided 3-D model is not adequate to provide a robust interpretation. Further studies with high density MT sites and additional geophysical datasets would be requested for an adequate interpretation, with the possibility of defining if this anomaly may be related to the pathways used by the asthenospheric mantle to reach the surface at the GVA.

6.5 Off profile anomalies, *A1* and *A2*

Outside the profiles (Fig. 3), two major anomalies, *A1* and *A2*, are observed to the north of the Central and Eastern Pyrenees MT Profiles, and between the eastern profile and the

Mediterranean Sea respectively. Although these regions are not well resolved in the MT model, the sensitivity tests suggest that the measured data are affected by the presence of low electrical resistivity values in these areas.

A1 is coincident with an anomalous decrease in the Bouguer anomaly, and with high velocity values (e.g. Chevrot et al., 2014; Souriau et al., 2008; see Figure S5 in the supplementary material for more detail). *A2* is coincident with regions where strong influence of the Mediterranean rifting is expected. Previous studies suggested crustal and lithospheric thinning at the eastern end of the Pyrenees, but no significant evidences were observed below the Eastern Pyrenees MT profile, implying that these variations probably occur in a short distance, between the Eastern Pyrenees MT profile and the Mediterranean Sea. *A2* could be associated with this sharp contrast related to the crustal and lithospheric thinning. Further studies with sites located directly on top of *A1* and *A2* will enable appropriate recovery of the associated structures (depth, shape and resistivity values), and provide a reasonable interpretation.

7. Conclusions

The results of our study interpreting new data form the Eastern Pyrenees MT profile and old data from Central Pyrenees MT profile by means of 3-D joint inversion of electromagnetic data (including ***Z***, ***T*** and ***H*** data) provide the first lithospheric-scale geoelectrical evidence of the tectonic scenario beneath the Central-Eastern Pyrenees. The main result of this study is the characterization of the non-continuity to the east of the major conductive anomaly observed previously beneath the Central and West-Central Pyrenees related to partial melting of the IBSLC. We also constrained the lateral extension of this region associated with partial melting only few km to the east of the Central Pyrenees MT profile. The lack of partial

melting below the Eastern Pyrenees MT profile was justified by lower amounts of muscovite and biotite in the IBSLC, which were key minerals for explaining the presence of partial melting below the West-Central and Central Pyrenees MT profiles. The higher electrical resistivity values of the lithospheric mantle below the Eastern Pyrenees MT profile than below the Central Pyrenees MT profile support the hypothesis of an heterogeneous Iberian plate with significant lateral variations inherited from the Variscan orogeny. The sensitivity tests performed to constrain the top of L2 and L3 structures suggest the possibility of lateral variations along the strike direction of the eLAB, with a north-dipping eLAB beneath the Central Pyrenees MT profile and a relatively flat eLAB beneath the Eastern Pyrenees MT profile. The relatively flat eLAB beneath the Eastern Pyrenees MT profile would be in agreement with the hypothesis of missing lithospheric root and orogenic collapse at the eastern end of the Pyrenean range. Finally, the two off-profile anomalies, *A1* and *A2*, and the L4 anomaly, suggest future areas of study where additional data is needed for a reliable interpretation. In particular, new data to the east of the actual Eastern Pyrenees MT profile will provide valuable information about the effects of the opening of the Mediterranean Sea to the onshore Pyrenean structures.

Acknowledgements

This research was funded by the Departament de Geodinàmicai Anàlisis de Conques (2009SRG1198) and the Departament d'Universitats, Investigació i Societat de la Informació de la Generalitat de Catalunya. We are grateful to Institute Cartogràfic i Geològic de Catalunya (ICGC) for providing complementary data used in this study, and to the landowners, la Xarxa de Parcs Naturals de Catalunya and l'Office National des Forêts, for allowing us to make measurements on their land. We thank INTERMAGNET for promoting high standards of magnetic observatory practice (www.intermagnet.org), and in particular we thank Fürstenfeldbruck (FUR) and Chambon la Fôret (CLF) magnetic observatories for the provided datasets in which the results of this paper relied on. Gary Egbert, Anna Kelbert and Naser Meqbel are very gratefully thanked for making their ModEM code available to the community. We are also grateful to the fieldwork assistants, especially to Lluís Guilà, Ivan Suñé, and Roger Llopart. Finally, the authors would like to thank Marion Jegen, the anonymous reviewer, and the Editor Ramon Carbonell for their very helpful suggestions and comments on the manuscript.

References

- Arthaud, F. and Séguret, M., 1981. Les structures pyrénéennes du Languedoc et du Golfe du Lion (Sud de la France) *Bull.Soc. Géol. Fr.* XXlII, 51-63.
- Baize, S., Cushing, M., Lemeille, F., Granier, T., Grellet, B., Carbon, D., Combes, P., Hibsch, C., 2002. Inventaire des indices de rup-ture affectant le Quaternaire, en relation avec les grandes structuresconnues en France métropolitaine et dans les régions limitrophes. *Mémoire hors série, Soc. Géol.Fr*.,175,142p.
- Beaumont, C., Muñoz, J.A., Hamilton, J. and Fullsack, P., 2000. Factors controlling the Alpine Evolution of the Central Pyrenees inferred from a comparison of observations and geodynamical models. *J. Geophys. Res.*, 105(B4), 8121–8145.
- Berdichevsky, M.N., Sokolova, E.Yu., Varentsov, Iv.,M., Rybin, A.K., Baglaenko, N.V., Batalev, V.Yu., Golubtsova, N.S., Matayukov, V.E. & Pushkarev, P.Yu., 2010. Geoelectric section of the Central Tien Shan: Analysis of magnetotelluric and magnetovariational Responses along the Naryn Geotransverse, *Physics of the Solid Earth*, 46(8), 679-697. doi:10.1134/S1069351310080057.
- Berdichevsky, M.N., Dmitriev, V. & Pozdnjakova, E.E., 1968. On two-dimensional interpretation of magnetotelluric soundings, *Geophys. J. Int.*, 133, 585–606.
- Blake et al., Henry, T., Muller M.R, Jones, A.G.,Moore, J.P., Murray, J., Campanyà, J., Vozar, J., Walsh, J., Rath, V 2016. Understanding hydrothermal circulation patterns at a low-enthalpy thermal spring using audio-magnetotelluric data: A case study from Ireland. *Journal of Applied Geophysics*,132, 1-16.
- Booker, J.R., 2014. The Magnetotelluric Phase Tensor: A Critical Review. *Surv. Geophys*. 35,7-40. doi:10.1007/s10712-013-9234-2
- Briais, A., Armijo, R., Winter, T., Tapponnier, P. & Herbecq, A., 1990. Morphological evidence for Quaternary normal faulting and seismic hazard in the eastern Pyrenees, *Annales Tectonicae*, IV, 19-42.

- Caldwell, G.T., Bibby, H.M., Brown, C., 2004. The Magnetotelluric Phase Tensor, *Geophys. J. Int.*, 158, 457–469.
- Campanyà, J., Ogaya, X., Jones, A.G., Rath, V., Vozar, J., and Meqbel, N, 2016. The advantages of complementing MT profiles in 3-D environments with geomagnetic transfer function and inter-station horizontal magnetic transfer function data: Results from a synthetic case study. *Geophysical Journal International*, 207, 1818–1836. doi: 10.1093/gji/ggw357.
- Campanyà, J., J. Ledo, P. Queralt, A. Marcuello, & A.G. Jones, 2014. A new methodology to estimate magnetotelluric (MT) tensor relationships: Estimation of Local transfer-functIons by Combining Inter-station Transfer-functions (ELICIT), *Geophy. J. Int.*, 198, 484-494, doi: 10.1093/gji/ggu147.
- Campanyà, J. 2013. Innovation of the magnetotlleuric method and its application to the characterisation of the Pyrenean lithosphere. PhD thesis. Universitat de Barcelona (UB). Supervisor: Dr. Juanjo Ledo.. http://www.tdx.cat/handle/10803/112702
- Campanyà, J., Ledo, J., Queralt, P., Marcuello, A., Liesa, M. & Muñoz, J.A. 2012. New geoelectrical characterization of a continental collision zone in the West- Central Pyrenees: Constraints from long period and broadband magnetotellurics. *Earth Planet. Sci. Lett.*, 333-334, 112-121.doi:10.1016/j.epsl.2012.018.
- Campanyà, J., Ledo, J., Queralt, P., Marcuello, A., Liesa, M. & Muñoz, J.A. 2011. Lithospheric characterization of the Central Pyrenees based on new magnetotelluric data. *Terra Nova*. 23, 213 - 219. doi: 10.1111/j.1365-3121.2011.01001.x .
- Cantwell, T., and Madden, T.R., 1960. Preliminary report on crustal magnetotelluric measurements. *Journal of Geophysical Research*. Letters to Editor. 10.1029/JZ065i012p04202
- Chave, A.D. and Thompson, D.J., 2004. Bounded influence estimation of magnetotelluric response functions. *Geophysical Journal International*, 157, 988-1006.
- Chave, A.D. & Jones, A.G., 1997. Electric and magnetic field galvanic distortion decomposition of BC87 data, *Journal of Geomagnetism and Geoelectricity*, 49, 767-789.
- Chave, A.D. & Smith, J.T., 1994. On electric and magnetic galvanic distortion tensor decompositions, *Journal of Geophysical Research:Solid Earth*, 99, 4669-4682.

- Chevrot, S., Sylvander, M., ; Diaz, J., Ruiz, M., Paul, A., and the PYROPE working Group. 2015. The Pyrenean architecture as revealed by teleseismic P-to-S converted waves recorded along two dense transects. *Geophysical Journal International*. 200, 1096–1107. doi: 10.1093/gji/ggu400.
- Chevrot, S., et al., 2014. High-resolution imaging of the Pyrenees and Massif Central from the data of the PYROPE and IBERARRAY portable array deployments, *J. Geophys. Res. Solid Earth*, 119, 6399–6420, doi:10.1002/2014JB010953.
- Choukroune and Ecors Team, 1989. The ECORS Pyrenean deep seismic profile: reflection data and the overall structure of the orogenic belt. *Tectonics*, 8, 23-39.
- Daignières, M., de Cabissole, B., Gallart, J., Him, A., Suriñiach, E., and M. Torné, M., 1989. Geophysical constraints on the deep structure along the ECORS Pyrenees Line, *Tectonics*, 8,5,1051-1058.
- ECORS-Pyrenees Team, 1988. The ECORS deep reflection seismic survey across the PyreÅLneÅL es. Nature, 331, 508–510.
- Egbert, G. D. & A. Kelbert, 2012. Computational Recipes for Electromagnetic Inverse Problems. *Geophys. J. Int*. 189, 251–267.doi: 10.1111/j.1365-246X.2011.05347.x
- Egbert, G.D. & Booker, J.R.: 1989. Multivariate analysis of geomagnetic array data 1, The response space, J. Geophys. Res., 94, 14,227–14,248.Egbert, G. D., & Kelbert, A., 2012. Computational recipes for electromagnetic inverse problems, *Geophys. J. Intern.*, 189(1), 251-267.
- Farquharson, C.G., Craven, J.A., 2009. Three-dimensional inversion of magnetotelluric data for mineral exploration: an example from the McArthur River uranium deposit, Saskatchewan, Canada. *Journal of Applied Geophysics* 68, 450-458.
- Friedrichs, B., 2003. Mapros, Magnetotelluric Processing Software (Metronix). User Manual.
- Fullea, J., 2017. On joint modelling of electrical conductivity and other geophysical and petrological observables to infer the structure of the lithosphere and underlying upper mantle. *Surveys in Geophysics* (Under review).
- Gallart, J., Díaz, J., Nercessian, A., Mauffret, A., Dos Reis, T., 2001. The eastern end of the Pyrenees: Seismic features at the transition to the NW Mediterranean. *Geophysical research Letters*, 28(11), 2277-2280 .

- Gamble, T.D., Clarke, J. & Goubau, W.M., 1979a. Magnetotellurics with a remote magnetic reference, *Geophys*, 44, 1, 53-68.
- Gamble, T.D., Clarke, J. & Goubau, W.M., 1979b. Error analysis for remote reference magnetotellurics: *Geophys*, 44, 959-968.
- Garrido, A. and Rios, L.M., 1972. Sintesis Geologica del Secundario y Terciario entre los rıos Cinca y Segre (Pirineo Central de la vertiente surpirenaica, provincias de Huesca y Lerida). Bol. Geol. Min., 83, 1–47.
- Glover, P.W.J., Pous, J., Queralt, P., Muñoz, A., Liesa, M. and Hole, M.J., 2000. Integrated two-dimensional lithospheric conductivity modelling in the Pyrenees using field-scale and laboratory measurements. Earth Planet. Sci. Lett., 178, 59–72.
- Gunnell, Y., M. Calvet, S. Brichau, A. Carter, J. P. Aguilar, and H. Zeyen, 2009. Low long-term erosion rates in high-energy mountain belts: Insights from thermo- and biochronology in the Eastern Europe, *Earth Planet. Sci. Lett*., 278, 208–218.
- Gunnell, Y., Zeyen, H. and Calvet, M., 2008. Geophysical evidence of a missing lithospheric root beneath the Eastern Pyrenees: Consequences for post-orogenic upflit and associated geomorphic signatures. *Earth and Planetary Science Letters*, 276, 302-313.
- Habibian, B.D. & Oskooi, B., 2014. A resolution comparison of horizontal and vertical magnetic transfer functions, J. Earth Space Phys., 40(3), 47–53.
- Jammes, S., Huismans, R.S., Muñoz, J.A., 2014. Lateral variation in structural style of mountain building: controls of rheological and rift inheritance, *Terra Nova*, 26 (3), 201-207.
- Jones, A. G. 2011, Distortion of magnetotelluric data: its identification and removal, in A. D. Chave and A. G. Jones, eds., The Magnetotelluric Method: Theory and Practice: Cambridge University Press.
- Jones, A.G., 1986. Parkinson's pointers' potential perfidy!, *Geophysical Journal of the Royal Astronomical Society*, 87, 1215-1224.
- Kelbert, A., Meqbel, N., Egbert, G. D., & Tandon, K., 2014. ModEM: A Modular System for Inversion of Electromagnetic Geophysical Data. *Computers & Geosciences*. 66,40-53. http://dx.doi.org/10.1016/j.cageo.2014.01.010.
- Lacan, P. & Ortuño, M., 2012. Active tectonics of Pyrenees: A review, J. Iberian Geol., 38, 9-30.

- Ledo, J., and Jones, A.G., 2005. Upper mantle temperature determined from combining mineral composition, electrical conductivity laboratory studies and magnetotelluric field observations: Application to the intermontane belt, Northern Canadian Cordillera. Earth and Planetary Science Letters, 236, 258-268.
- Ledo, J., 2005. 2-D versus 3-D magnetotelluric data interpretation, *Surv. Geophys*., 26, 511–543.
- Ledo, J., Ayala, C., Pous, J., Queralt, P., Marcuello, A. and Muñoz, A., 2000. New geophysical constrains on the deep structure of the Pyrenees. *Geophysical Research Letters*, 27, 1037-1040.
- Ledo, J., 1996. Aplicación del método magnetotelúrico al estudio de la estructura litosférica de los Pirineos, PhD, Universitat de Barcelona, Spain, 196 pp.
- Lewis, C., Vergés, J., and Marzo, M., 2000. High mountains in a zone of extended crust: Insights into the geodynamic evolution of northeastern Iberia, *Tectonics*, 19, 86-102.
- Macquet, M., Paul, A., Pedersen, H.A., Villase˜nor, A., Chevrot, S., Sylvander, M.,Wolyniec, D. & PYROPEWorking Group, 2014. Ambientnoise tomography of the Pyrenees and surrounding regions: inversion for a 3-D Vs model in the presence of a very heterogeneous crust, *Geophys. J. Int*., 199, 402–415.
- Martí, J., Planagumà, L., Geyer, A., Canal, E., & Pedrazzi, D., 2011. Complex interaction between Strombolian and phreatomagmatic eruptions in the Quaternary monogenetic volcanis of the Catalan Volcanic Zone (NE of Spain).*Journal of Volcanology and Geothermal Research*, 201(1), 178-193.
- Martí, J., Mitjavila, J., Roca, E., and Aparicio, A., 1992. Cenozoic magmatism of the Valencia trough (Western Mediterranean): Relationship between structural evolution and vulcanism: *Tectonophysics*, 203, p. 145-165.
- Martí, A., Queralt, P., Roca, E., Ledo, J. and Galindo-ZaldıÅLvar, J., 2009a. Geodynamic implications for the formation of the Betic–Rif orogen from magnetotelluric studies. J. Geophys. Res., 114, B01103, doi:10.1029/2007JB005564.
- Meqbel, N.M; Egbert, G.D., Wannamaker, P.E., Kelbert, A., Schultz, A., 2014. Deep electrical resistivity structure of the northwestern U.S. derived from 3-D inversion of USArray magnetotelluric data. *Earth and Planetary Science Letters*, 402, 290-304. doi:10.1016/j.epsl.2013.12.026.

- Muñoz, J. A., 2002. The Pyrenees, in The Geology of Spain, edited by W. Gibbons and T. 625 Moreno, pp. 370-385, *Geological Society of London*, London.
- Muñoz, J.A., 1992. Evolution of a continental collision belt: ECORS-Pyrenees crustal balanced 622 cross-section. In: K.R. McClay (Editor) In: Thrust Tectonics. Chapman & Hall, London, p. 623 235-246.
- Neska, A., Reda, J. T., Neska, M. L., and Sumaruk, Y. P.: On the relevance of source effects in geomagnetic pulsations for induction soundings, Ann. Geophys., 36, 337-347, https://doi.org/10.5194/angeo-36-337-2018, 2018.
- Nercessian, A., Mauffret, A., Dos Reis, A.T., Vidal, N., Gallart, J. and Diaz, J.,2001. Deep reflection seismic images of the crustal thinning in the eastern Pyrenees and western Gulf of Lion, *J. Geodyn*.3, 1, 2, 211-225.
- Neumann, E.R., Martí, J., Mitjavila, J., and Wulff-Pedersen, E., 1999. Origin and implications of mafic xenoliths associated with Cenozoic extension-related volcanism in the València Trough, NE Spain: *Mineralogy and Petrology*, *65*, p. 113-139
- Neves, A, S de S, 1957. The Generalized Magneto-Telluric Method. Unpubl. Ph.D. thesis, MIT.
- Olivet, J.L., 1996. La cinematique de la plaque Iberique. Bull. Centres Res. Explor. Prod. Elf Aquitanie 20, 131-195.
- Parkinson, W.D., 1962. The influence of the continents and oceans on geomagnetic variations. *Geophys. J.R. Astron. Soc*., 80, 177-194.
- Perea, H., 2009. The Catalan seismic crisis (1427 and 1428; NE Iberian Peninsula): Geological sources and earthquake triggering, *J. Geodynamics*, 47, 259-270.
- Pous, J., Ledo, J., Marcuello, A. and Daignières, M., 1995a. Electrical resistivity model of the crust and upper mantle from a magnetotelluric survey through the central Pyrenees. *Geophys. J. Int*., 121, 750–762.
- Pous, J., Muñoz, A., Ledo, J. and Liesa, M., 1995b. Partial melting of subducted continental lower crust in the Pyrenees. *J. Geol. Soc. London*, 152, 217–220.
- Rigo A., Vernant, P., Feigl, K.L., Goula, X., Khazaradze, G., Talaya, J., Morel, L., Nicolas, J., Baize, S., Chery, J., Sylvander, M., 2015. Present-day deformation of the Pyrenees revealed by GPS surveying and earthquake focal mechanisms until 2011. *G. J. Int.*, 201, 947-964, 10.1093/gji/ggv052
- Roca, E., Muñoz, J. A., Ferrer, O., Ellouz, N., 2011. The role of the Bay of Biscay Mesozoic extensional structure in the configuration of the Pyrenean orogen:

Constraints from the MARCONI deep seismic reflection survey. *Tectonics*, 30, TC2001.

- Roca, E., M. Sans, L. Cabrera, and M. Marzo, 1999, Oligocene to Middle Miocene evolution of the central Catalan margin (northwestern Mediterranean): Tectonophysics, v. 315, no. 1-4, p. 209–229, doi:10.1016/S0040-1951(99)00289-9.
- Roca, E., and Guimerà, J., 1992. The Neogen structure of the eastern Iberian margin: structural constraints on the crustal evolution of the València trough (Western Mediterranean). *Tectonophysics*, 203, 203-218.
- Rokityanski, I.I. 1961. On the application of the magnetotelluric method to anisotropic and inhomogeneous masses. *Izvestia*, 11, 1607-1613.
- Rosell, O., Martí, A., Marcuello, A., Queralt, P., Roca, E., and Campanyà, J., 2011. Deep electrical resistivity structure of the northern Gibraltar Arc (western Mediterranean): evidence of lithospheric slab break-off. *Terra Nova*, 23, 179-186.
- Rosenbaum, G., Lister, G. S. and Duboz, C. 2002. Reconstruction of the tectonic evolution of the western Mediterranean since the Oligocene. In:Rosenbaum, G. and Lister, G. S. 2002. Reconstruction of the evolution of the Alpine-Himalayan Orogen. *Journal of the Virtual Explorer*, 8, 107 - 130.
- Roure, F., Choukroune, P., Berastegui, X., Muñoz, J. A., Villien, A. M., Thereon, P., Bareyt, M., Séguret, M., Cámara, P., and Déramond, J., 1989, ECORS deep seismic data and balanced cross sections: Geometric constraints on the evolution of the Pyrenees, *Tectonics*, 8, no. 1, p. 41-50.
- Sasaki, Y. & Meju, M.A., 2006. Three-dimensional joint inversion for magnetotelluric resistivity and static shift distributions in complex media, *Journal of Geophysical Research-Solid Earth*, 111, 11.
- Schmucker, U., 1970. Anomalies of geomagnetic variations n the Southwestern United States. *J. Geomagn. Oceanogr*., Univ. of California Press, Berkeley.
- Selway, K., Hand, M., Heinson, G.S. and Payne, J.L., 2009. Magnetotelluric constrains on subduction polarity: reversing reconstruction models for Proterozoic Australia. Geology, 37, 799–802, doi:10.1130/G30175A.1.
- Séranne, M., A. Benedicto, P. Labaum, C. Truffert, and G. Pascal, 1995, Structural style and evolution of the Gulf of Lion Oligo-Miocene rifting: Role of the Pyrenean orogeny: Marine and Petroleum Geology, v. 12, no. 8, p. 809–820.

- Siripunvaraporn, W. & Egbert, G., 2009. WSINV3DMT: vertical magnetic field transfer function inversion and parallel implementation, Phys. Earth planet. Inter., 173, 317–329.
- Sokolova, E.Yu., Varentsov, Iv.M. & BEAR Working Group, 2007. Deep array electromagnetic sounding on the baltic shield: external excitation model and implications for upper mantle conductivity studies, Tectonophysics, 445, 3–25.
- Souriau, A., Chevrot, S. and Olivera, C, 2008. A new tomographic image of the Pyrenean lithosphere from teleseismic data. *Tectonophysics,* 460, 206-214.
- Soyer, W. & Brasse, H., Investigation of anomalous magnetic field variations in the central Andes of N Chile and SW Bolivia. *Geophysical Research. Letters*, 2001, 28 (15):3023–3026.
- Stampfli, G. M., and Hochard, C., 2009, Plate tectonics of the Alpine realm: Geological Society, London, Special Publications, v. 327, no. 1, p. 89–111, doi:10.1144/SP327.6.
- Teixell, A., 1998. Crustal structure and orogenic material budget in the west central Pyrenees. *Tectonics*, 17, 395-406.
- Türkoğlu, E., Unsworth, M., Çağlar, I., Tuncer, V. and Avsar, Ü., 2008. Lithospheric structure of the Arabia-Eurasia collision zone in eastern Anatolia: magnetotelluric evidence for widespread weaking by fluids? Geology, 36, 619–622, doi:10.1130/G24683A.1.
- Unsworth, M., 2009. Magnetotelluric studies of active continent–continent collisions. Surv. Geophys., 31, 137–161.
- Vacher, P. and Souriau, A., 2001. A threedimensional model of the Pyrenean deep structure based on gravity modelling, seismic images and petrological constraints. Geophys. J. Int., 145, 460–470.
- Varentsov, Iv.M., 2015a. Methods of joint robust inversion in MT and MV studies with application to synthetic datasets, in Electromagnetic Sounding of the Earth's Interior: Theory, Modeling, Practice, pp. 191–229, ed. Spichak, V.V., Elsevier.
- Varentsov, Iv.M., 2015b. Arrays of simultaneousEMsoundings: design, data processing, analysis, and inversion, in Electromagnetic Sounding of the Earth's Interior: Theory, Modeling, Practice, pp. 271–299, ed. Spichak, V.V., Elsevier
- Vergés, J., Fernàndez, M. & Martínez, A. 2002. The Pyrenean orogen: pre-, syn-, and post-collisional evolution. In: Rosenbaum, G. and Lister, G. S. 2002. Reconstruction

of the evolution of the Alpine-Himalayan Orogen. *Journal of the Virtual Explorer*, 8, 55 - 74.

- Vergés, J., Millán, H., Roca, E., Muñoz, J. A., Marzo, M., Cirés, J., den Bezemer, T., Zoetemeijer, R., and Cloetingh, S., 1995. Eastern Pyrenees and related foreland basins: Pre-, syn- and post-collisional crustal-scale cross-sections., in Cloetingh, S., Durand, B., and Puigdefàbregas, C., eds., *Marine and Petroleum Geology*, p. 903-916.
- Vielzeuf, D., 1984. Relations de phases dans les facies granulite et implications géodynamiques. L'éxemple des granulites des Pyrénéés. Thèse Doctorat d'État, Université Blaise Pascal, Clermont- Ferrand, France, 288 pp.
- Vidal, N., Gallart, J., and Dañobeitia, J. J., 1998, A deep seismic crustal transect from the NE Iberian Peninsula to the western Mediterranean: *Journal of Geophysical Research*, 103, no. 6, p. 12,381-12,396.
- Wei, W.B., Unsworth, M., Jones, A., Booker, J., Tan, H.D., Nelson, D., Chen, L.S., Li, S.H., Solon, K., Bedrosian, P., Jin, S., Deng, M., Ledo, J., Ray, D. and Roberts, B., 2001. Detection of widespread fluids in the Tibetan crust by magnetotelluric studies. Science, 292, 716–718.
- Wiese, H., 1962. Geomagnetische Tiefentellurik. *Geophys. Pure Appl*. 52, 83-103.

Figure Captions

Figure 1 Location of the MT sites on a topographic map of the Pyrenees. E2 site used as a reference site for the ***H*** responses. EB, Ebro Basin; SPTS, South Pyrenean Thrust Sheets; AX, Axial Zone; NPF, North Pyrenean Fault; NPTS, North Pyrenean Thrust Sheets; AB, Aquitaine Basin. Thin black lines divide the main geological units of the region. Gray lines indicate the locations of the seismic profiles.

Figure 2 a) Electrical resistivity model below the Central and Eastern Pyrenees MT profiles. *L1 -L4* labels showing the location of the main geoelectrical structures. Red inverted triangles at the top of the models show the location of the MT sites. NPF: North Pyrenean Fault used as a reference point; GVA: Garrotxa Volcanic Area. b) nRms between data and model responses for ***Z*** (black), ***T*** (red) and ***H*** (green) datasets at the Central and Eastern Pyrenees MT sites.

Figure 3 Horizontal slices of the electrical resistivity model at different depths with the topography and major geological structures superimposed on top. At the slices at 20 km depth *A1* and *A2* are major anomalies out of the profiles. White rectangles at the slices at 30 km and 50 km depth represent the tests performed studding the eastern propagation of the conductive anomaly associated with the IBSLC (Continuous white lines are eastern edges that agree with the data; white dashed lines are tests performed propagating *L1* anomaly to the east that does not agree with the data acquired at the surface).

Figure 4 a) Topography along the Central and Eastern Pyrenees MT profiles including points at +/- 0.4º longitude. b) Bouguer anomaly along the Central and Eastern Pyrenees MT profiles including points at +/- 0.4º longitude. c) White circles are the location of the Earthquakes below the MT profiles. Black line superimposed to the Central Pyrenees MT model is the geological interpretation based on the existent geological models (Muñoz,

992). Black dashed lines superimposed to the Eastern Pyrenees MT model are the dipper structures of the Central Pyrenees geological interpretation using NPF as a reference point. Yellow dashed lines are the upper and lower boundaries of the eLAB from the sensitivity test. Yellow arrow indicates the possible pathways used by the basaltic magma to reach the surface associated with L4. Red inverted triangles are the location of the sites. NPF: North Pyrenean Fault used as a reference point; GVA: Garrotxa Volcanic Area.

Figure 5 a) Horizontal slice of the P velocity model from Chevrot et al., 2014 with the location of the MT sites acquired in the Central and Eastern Pyrenees (white circle). b) Comparison between Common Conversion Point (CCP) stack section from Chevrot et al., 2015 from the Central Pyrenees and the location of the L1 anomaly constrained below the Central Pyrenees (green dashed lines). Black dashed lines were associated with the Moho. NPF: North Pyrenean Fault.

Highlights

- New electrical resistivity model of the Central – Eastern Pyrenean lithosphere.
- Electrical imaging of presence and absence of lower crust melting processes
- Heterogeneous Iberian plate with lateral variations inherited from the Variscan Orogeny
- European-Iberian lithosphere–asthenosphere boundary transition: new constrain of a missing lithospheric root beneath the Eastern Pyrenees.
- 3-D joint inversion of electromagnetic geophysical responses (***Z***+***T***+***H***)

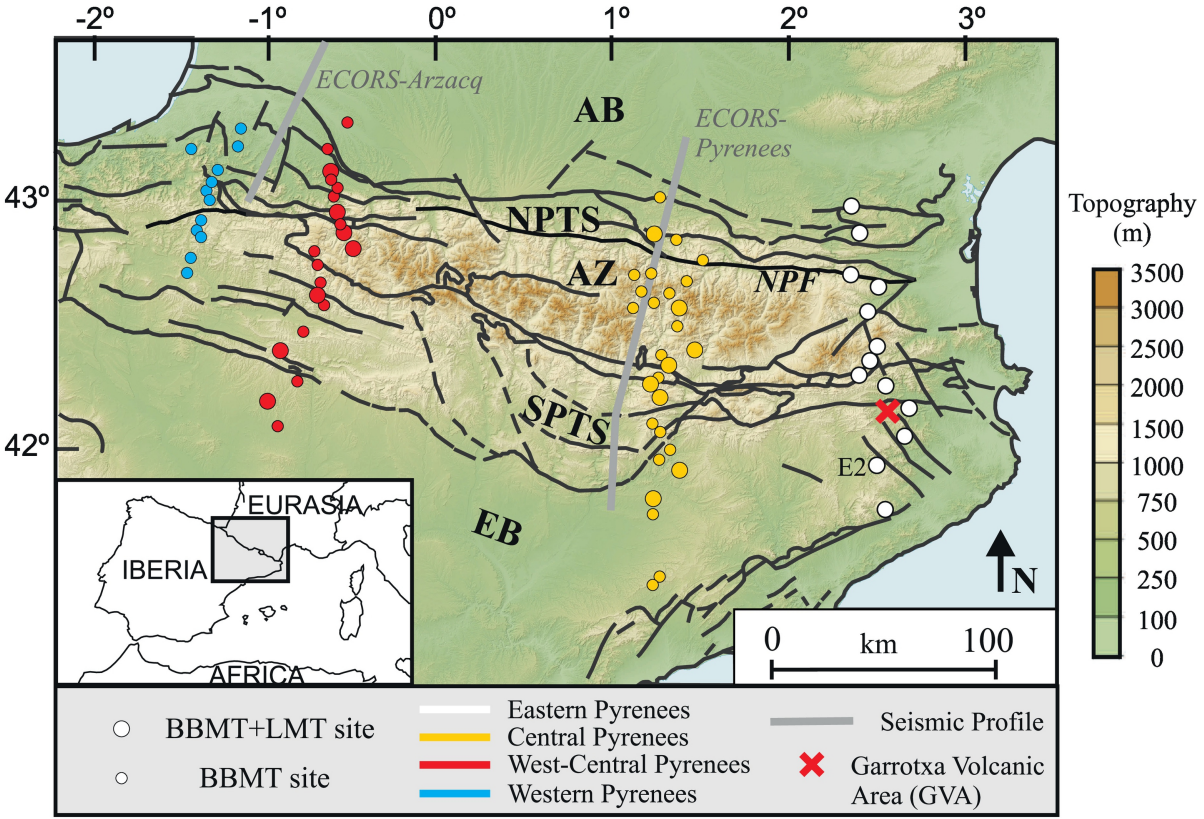
-2º
-1º
0º
1º
2º
3º
43º
42º
ECORS-Arzacq
ECORS-Pyrenees
AB
NPTS
AZ
NPF
SPTS
EB
E2
EURASIA
IBERIA
AFRICA
N
0
km
100
Topography (m)
3500
3000
2500
2000
1500
1000
750
500
250
100
0
BBMT+LMT site
BBMT site
Eastern Pyrenees
Central Pyrenees
West-Central Pyrenees
Western Pyrenees
Seismic Profile
Garrotxa Volcanic Area (GVA)

Figure 1

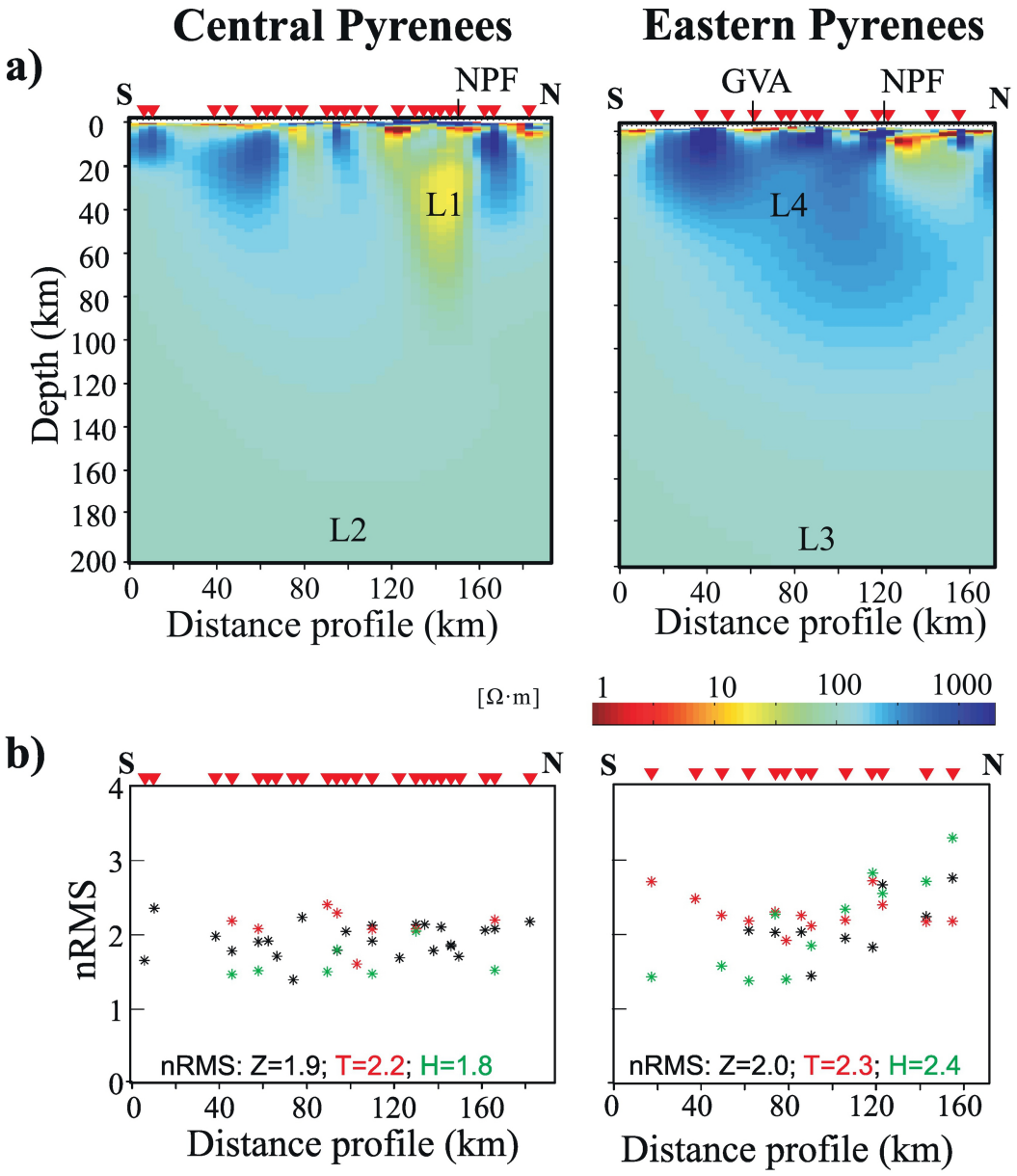
a)
Central Pyrenees
Eastern Pyrenees
S
N
NPF
GVA
L1
L2
L3
L4
Depth (km)
0
20
40
60
80
100
120
140
160
180
200
0
40
80
120
160
Distance profile (km)
[Ω·m]
1
10
100
1000
b)
nRMS
0
1
2
3
4
nRMS: Z=1.9; T=2.2; H=1.8
nRMS: Z=2.0; T=2.3; H=2.4

Figure 2

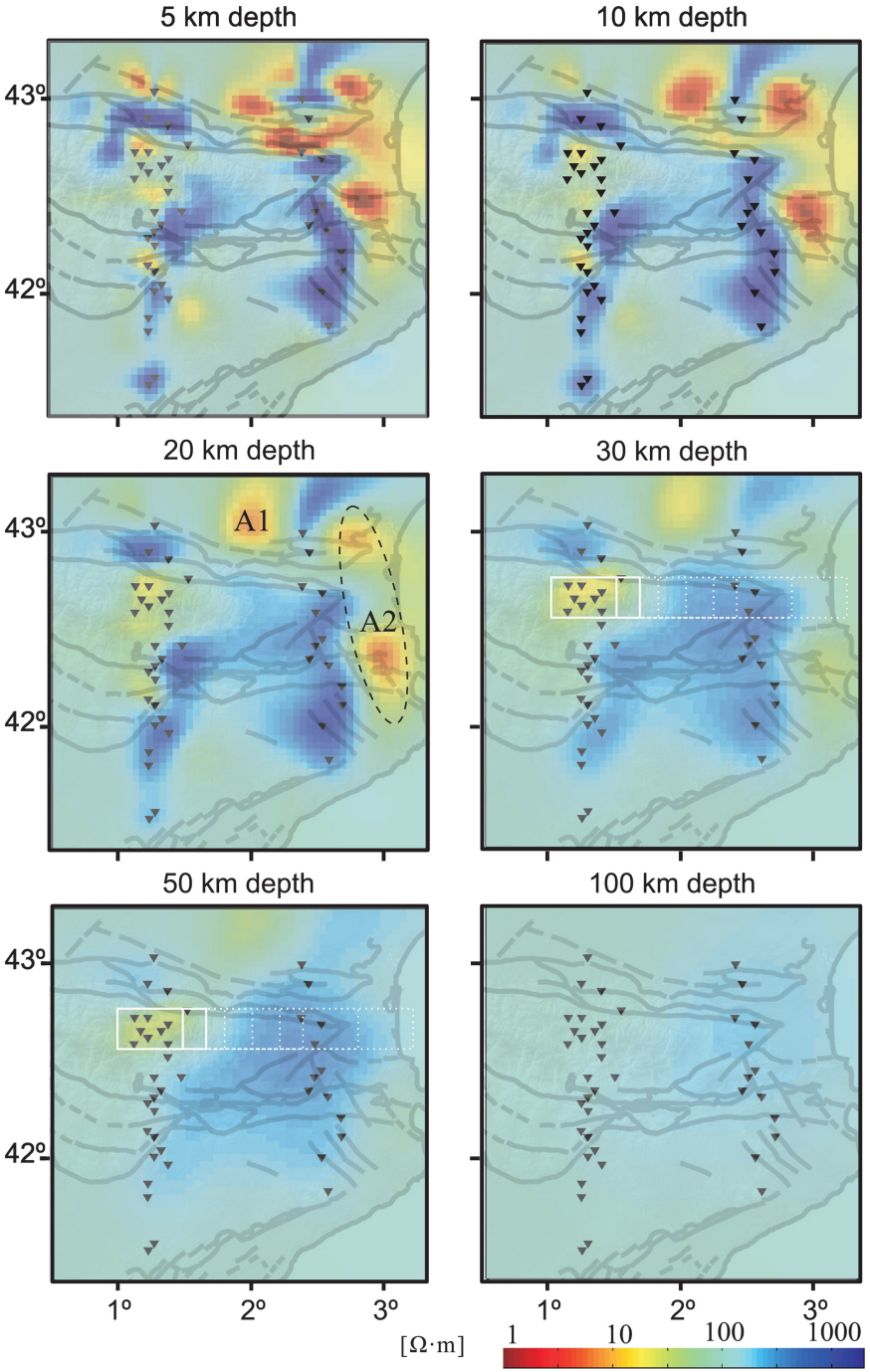
Horizontal slices
5 km depth
10 km depth
20 km depth
30 km depth
50 km depth
100 km depth
43º
42º
A1
A2
1º
2º
3º
[Ω·m]
1
10
100
1000

Figure 3

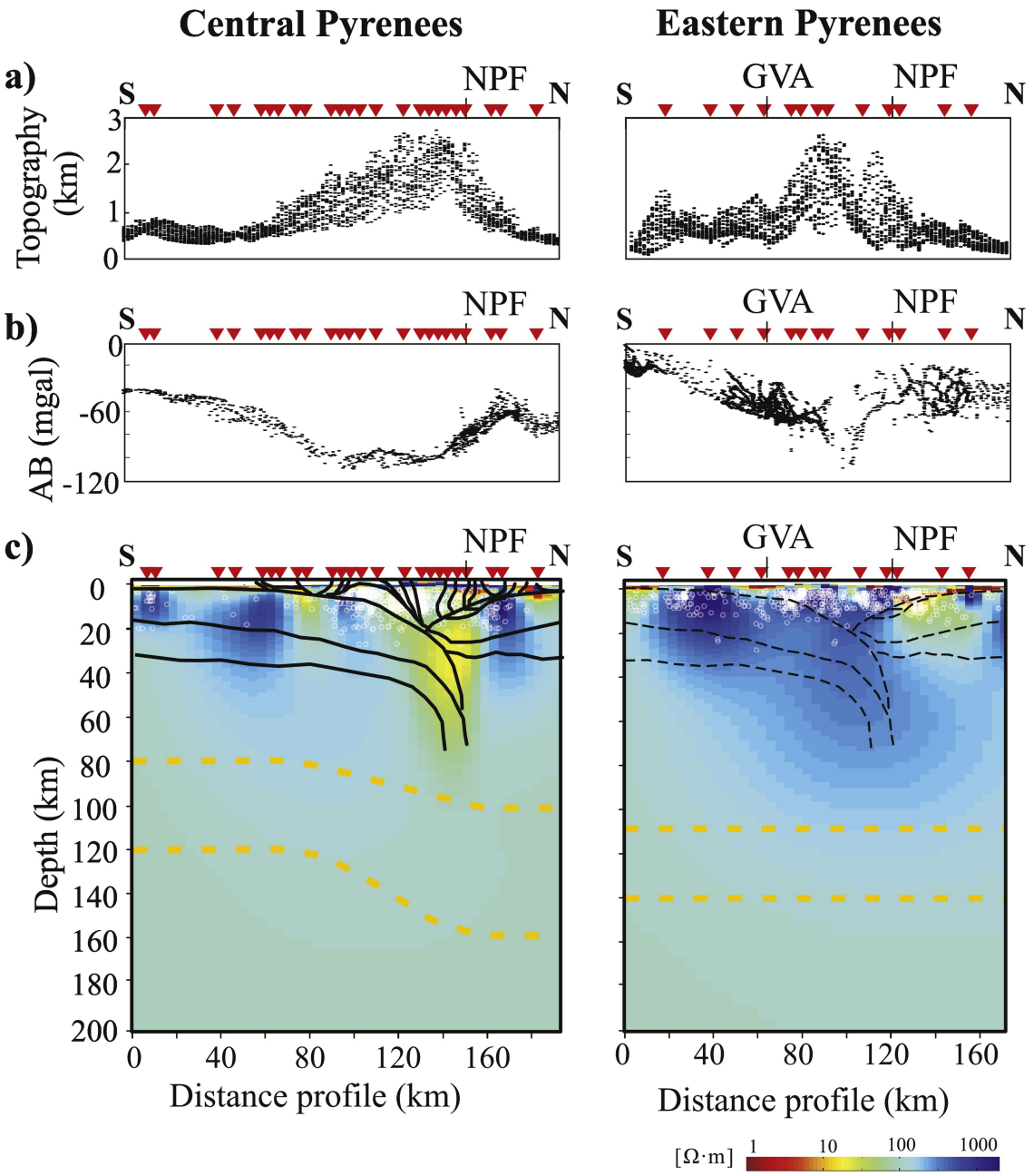
Central Pyrenees
Eastern Pyrenees
a)
b)
c)
S
N
NPF
GVA
Topography (km)
AB (mgal)
Depth (km)
Distance profile (km)
[Ω·m]
1
10
100
1000

Figure 4

a) P_velocity Model *(Modified from Chevrot et al., 2014)*

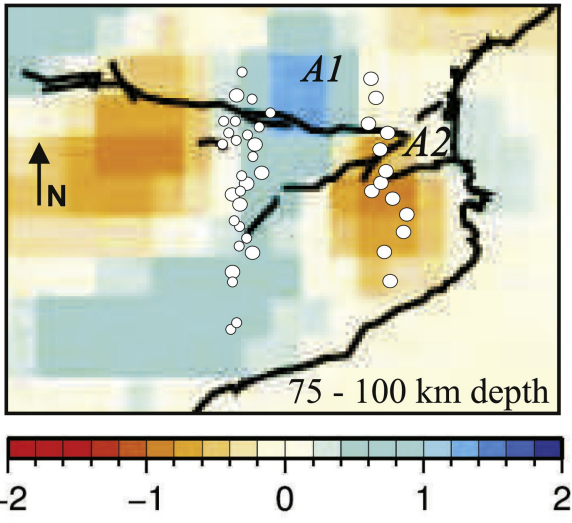

b) CCP stack section (*Modified from Chevrot et al., 2015*)

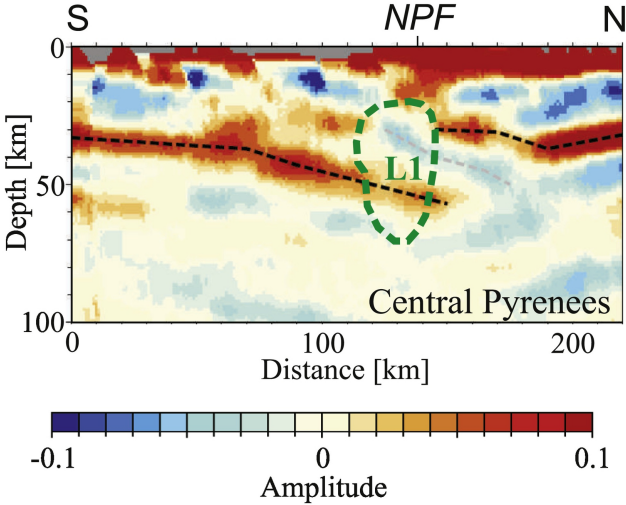

Figure 5